

An Artificial Z-Scheme Constructed from Dye-Sensitized Metal Oxide Nanosheets for Visible Light-Driven Overall Water Splitting

Takayoshi Oshima, Shunta Nishioka, Yuka Kikuchi, Shota Hirai, Kei-ichi Yanagisawa, Miharuru Eguchi, Yugo Miseki, Toshiyuki Yokoi, Tatsuto Yui, Koji Kimoto, Kazuhiro Sayama, Osamu Ishitani, Thomas E. Mallouk,* and Kazuhiko Maeda*



Cite This: <https://dx.doi.org/10.1021/jacs.0c02053>



Read Online

ACCESS |



Metrics & More

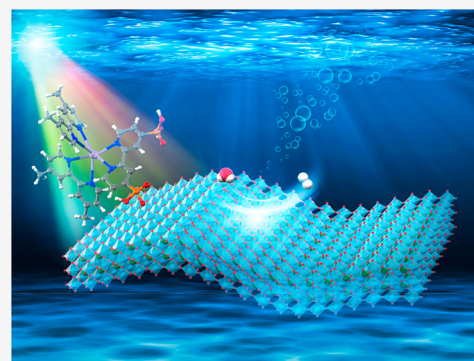


Article Recommendations



Supporting Information

ABSTRACT: Sensitization of a wide-gap oxide semiconductor with a visible-light-absorbing dye has been studied for decades as a means of producing H₂ from water. However, efficient overall water splitting using a dye-sensitized oxide photocatalyst has remained an unmet challenge. Here we demonstrate visible-light-driven overall water splitting into H₂ and O₂ using HCa₂Nb₃O₁₀ nanosheets sensitized by a Ru(II) tris-diimine type photosensitizer, in combination with a WO₃-based water oxidation photocatalyst and a triiodide/iodide redox couple. With the use of Pt-intercalated HCa₂Nb₃O₁₀ nanosheets further modified with amorphous Al₂O₃ clusters as the H₂ evolution component, the dye-based turnover number and frequency for H₂ evolution reached 4580 and 1960 h⁻¹, respectively. The apparent quantum yield for overall water splitting using 420 nm light was 2.4%, by far the highest among dye-sensitized overall water splitting systems reported to date. The present work clearly shows that a carefully designed dye/oxide hybrid has great potential for photocatalytic H₂ production, and represents a significant leap forward in the development of solar-driven water splitting systems.



INTRODUCTION

Growing energy demands and rising environmental concerns drive humanity to replace within the next few decades the use of CO₂-emitting fossil fuels with sustainable and clean energy sources. Dye-sensitized H₂ evolution from wide band gap semiconductors has been studied for decades as a potential way to generate renewable H₂ from water with visible light, and was proposed by Gerischer at the dawn of research in photoelectrochemistry.¹ In a dye-sensitized system, water splitting can be initiated by electron injection from an excited-state dye molecule into the conduction band of a semiconductor (Figure 1A). The injected electron then migrates to a catalytically active site such as a Pt nanoparticle to evolve H₂, while the oxidized dye is reduced by an electron donor to regenerate its ground state, completing the catalytic half-cycle. In parallel with these forward processes, backward electron transfer reactions, such as reduction of oxidized dye and/or electron donor by electrons in the conduction band, can also take place. Therefore, promoting the forward reaction, as well as retarding the back reaction, is important to improving the overall efficiency.

So far, many studies have been done, focusing on the development of efficient dye sensitizers,^{2–7} wide-gap semiconductor supports,^{8–14} and H₂-evolving catalysts.^{15,16} Spectroscopic studies have also provided mechanistic insight into dye-sensitized systems.^{17–21} However, most of the reported

dye-sensitized systems require a sacrificial electron donor such as ethylenediaminetetraacetic acid or triethanolamine for H₂ evolution to proceed at a measurable rate, and systems that can utilize a reversible electron donor (ideally water) are limited.^{8,9,17,22} To realize a nonsacrificial system (i.e., an artificial photosynthetic scheme in which the standard Gibbs free energy change is positive) through dye-sensitized H₂ evolution, suppressing back reaction(s) that can occur at the H₂ evolution site is a key because the oxidized form of a reversible electron donor can be easily reduced, hindering H₂ evolution.²² Visible-light photolysis of hydrogen iodide (HI) into H₂ and I₃⁻ has been demonstrated using photolysis of dye-sensitized, layered bulk H₂K₂Nb₆O₁₇, in which a H₂-evolution Pt cocatalyst was selectively deposited in the interlayer galleries.^{8,9,17} In that study, reduction of I₃⁻, which was produced as the result of oxidation of I⁻, was prevented by confining the H₂ evolution catalyst (i.e., Pt nanoparticles) to interlayer sites that were inaccessible to anions. Later on, Abe et al. reported overall water splitting using organic dye-

Received: February 20, 2020

Published: April 13, 2020



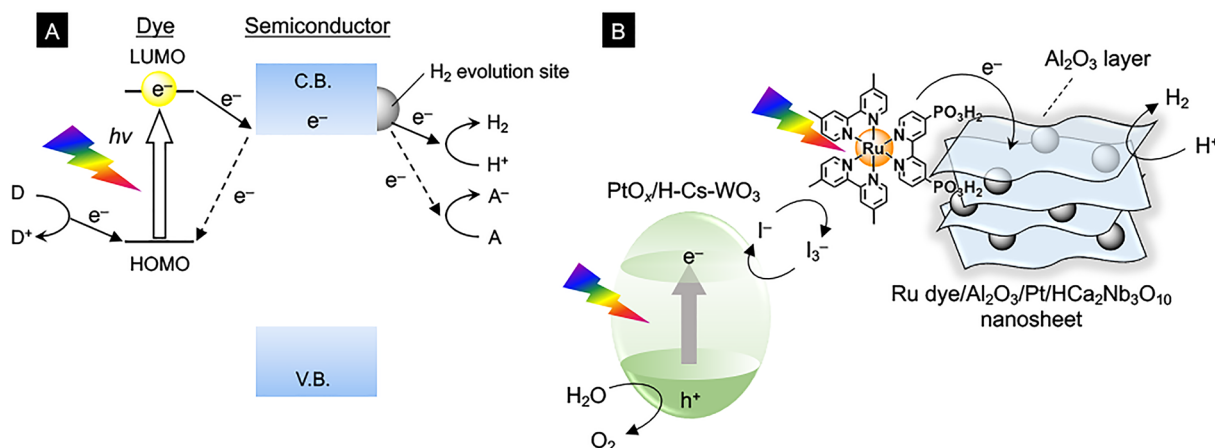


Figure 1. (A) Electron transfer mechanism of a hydrogen-evolving dye-sensitized photocatalyst. C.B.: conduction band, V.B.: valence band, HOMO: highest occupied molecular orbital, LUMO: lowest unoccupied molecular orbital, D: electron donor, D⁺: oxidized electron donor, A: electron acceptor, A⁻: reduced electron acceptor. Solid and broken arrows represent forward and back electron transfers, respectively. (B) Schematic picture of Z-scheme water splitting using Ru dye-sensitized Al₂O₃/Pt/HCa₂Nb₃O₁₀ nanosheets and PtO_x/H-Cs-WO₃.

sensitized H₂K₂Nb₆O₁₇ together with a water oxidation photocatalyst.²² However, the efficiencies attained in these nonsacrificial systems remain low, and thus new strategies for controlling forward and back reaction rates are needed.

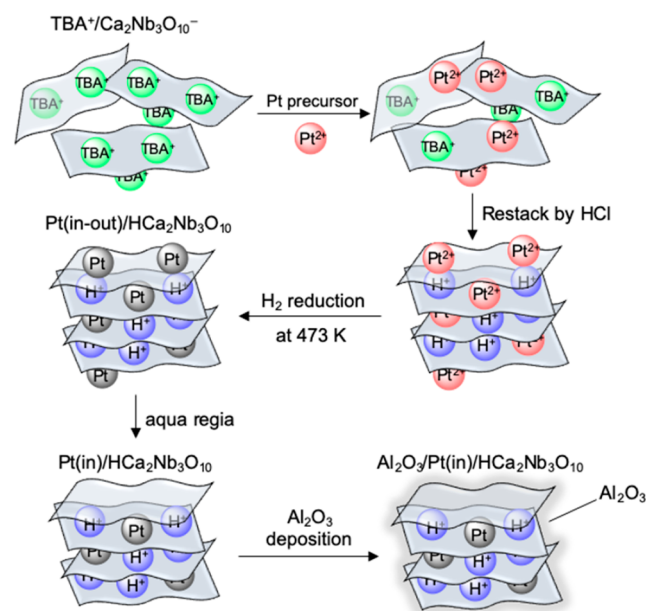
Metal oxide nanosheets are two-dimensional (1–2 nm thick) single crystals with lateral dimensions that are typically in the range of several hundreds of nm to a few μm .²³ The anisotropic structure, single-crystalline texture, and high surface area of these nanosheets have been shown to be beneficial for dye-sensitized H₂ evolution in terms of rapid electron transport through the semiconductor to H₂ evolution sites and the adsorption of photosensitizers.²⁴ Here, we report efficient dye-sensitized overall water splitting using modified HCa₂Nb₃O₁₀ nanosheets sensitized by a Ru(II) tris-diimine complex in a Z-scheme system with a WO₃-based O₂ evolution photocatalyst and an I₃⁻/I⁻ redox mediator (Figure 1B). We found that deposition of aluminum species on HCa₂Nb₃O₁₀ nanosheets was essential to boosting visible light-driven overall water splitting, and the working mechanism was elucidated by transient absorption spectroscopy.

RESULTS AND DISCUSSION

Preparation of Al₂O₃-Deposited, Pt-Intercalated HCa₂Nb₃O₁₀ Nanosheets. Pt nanoclusters were first deposited as H₂-evolution sites on restacked HCa₂Nb₃O₁₀ nanosheets by a method developed earlier in our group,²⁵ with some modifications (the detailed preparation procedure is described in the Experimental Section). At this stage, Pt was deposited both in the interlayer galleries and on the external surface of restacked HCa₂Nb₃O₁₀ [referred to as Pt(in-out)/HCa₂Nb₃O₁₀; see Scheme 1]. The Pt(in-out)/HCa₂Nb₃O₁₀ was then stirred in a boiling aqua regia (a mixed solution of concentrated HNO₃ and HCl 1:3 v/v) to dissolve Pt on the external surface [referred to as Pt(in)/HCa₂Nb₃O₁₀]. The removal of the externally deposited Pt was confirmed by a H₂-O₂ recombination experiment (see Figure S1 for detail). Results of the physicochemical characterization of the as-prepared Pt(in)/HCa₂Nb₃O₁₀ nanosheets are included in the SI (Figure S2–S6).

Pt(in)/HCa₂Nb₃O₁₀ was then further modified with aluminum species by a sol-gel method. Note that this

Scheme 1. Synthetic Scheme for Pt Intercalated HCa₂Nb₃O₁₀ Restacked Nanosheets



modification did not change the morphological features of Pt(in)/HCa₂Nb₃O₁₀ (Figure S6). The Al-2s XPS spectrum confirmed the deposition of aluminum species on the surface of Pt(in)/HCa₂Nb₃O₁₀ (Figure S7), with a peak binding energy of 118.8 eV. The value is close to that of Al₂O₃.²⁶ The surface atomic ratio of Al/Nb calculated from the XPS peak areas was 0.1. However, we could not eliminate the possible presence of hydrated phases (e.g., AlOOH) and/or Al(OH)₃, since it is difficult to differentiate Al₂O₃ and Al(OH)₃ by XPS.²⁷ Nevertheless, FT-IR spectroscopy indicated the absence of AlOOH and Al(OH)₃ on the surface of the Pt(in)/HCa₂Nb₃O₁₀ nanosheets (Figure S8). Therefore, it is likely that the deposited aluminum species was Al₂O₃, rather than AlOOH or Al(OH)₃.

Energy dispersive X-ray spectroscopy (EDS) analysis in scanning transmission electron microscopy (STEM) measurements also confirmed the existence of aluminum species after

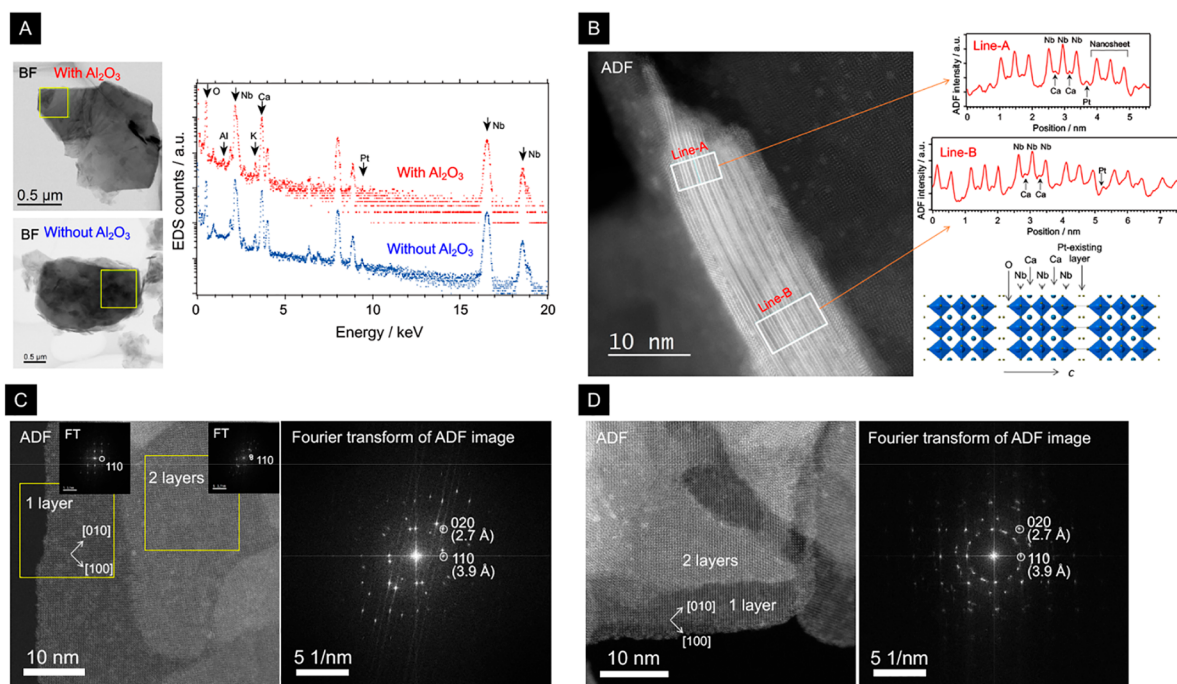


Figure 2. Results of STEM observations. (A) EDS analyses for Pt(in)/HCA₂Nb₃O₁₀ nanosheets with and without Al₂O₃ modification. (B) ADF image and line profiles for Al₂O₃/Pt(in)/HCA₂Nb₃O₁₀ nanosheets. Crystal structure of HCA₂Nb₃O₁₀·0.5H₂O (ICSD code: 246002) projected along [110] is also shown. Panels (C) and (D) show ADF images of Pt(in)/HCA₂Nb₃O₁₀ nanosheets with and without Al₂O₃ modification, respectively. Fourier transforms of the ADF images indicate that there is no crystalline component in the sample except for the HCA₂Nb₃O₁₀ nanosheets.

Al₂O₃ deposition (ca. 0.2 wt %), whereas no aluminum was detected before Al₂O₃ deposition (Figure 2A). STEM observations also suggested the presence of Pt species between nanosheets (Figure 2B), which is in line with the concept of catalyst preparation shown in Scheme 1. The amount of Pt deposited was estimated from EDS analysis to be approximately 0.3–0.4 wt %. On the other hand, no noticeable morphological changes were observed in STEM images regardless of Al₂O₃ deposition (Figures 2C and D). Moreover, Fourier transforms of high resolution STEM images of Al₂O₃/Pt(in)/HCA₂Nb₃O₁₀ exhibited only reciprocal lattice spots corresponding to HCA₂Nb₃O₁₀ nanosheets (Figure 2C), indicating that the deposited Al₂O₃ was amorphous.

Adsorption, Light-Absorption, and Emission Properties of Ru(II) Dye Sensitizers on HCA₂Nb₃O₁₀ Nanosheets. It is known that emission from excited Ru(II) tris-imine complexes is efficiently quenched by molecular O₂,²⁸ which is produced together with H₂ in photocatalytic overall water splitting. Quenching of the excited state by O₂ can compromise the efficiency of electron injection, and therefore the Ru(II) dye should be designed to minimize its reactivity with O₂.

Here we employed [Ru(4,4'-(CH₃)₂-bpy)₂(4,4'-(PO₃H₂)₂-bpy)]²⁺ (bpy = 2,2'-bipyridine), abbreviated as RuP (see Figure 1B) as a visible-light photosensitizer. The introduction of phosphonic acid groups to the bpy ligands enables strong anchoring to the metal oxide surface,^{4,5,12} while the electron withdrawing effect of the phosphonic acid, as well as the electron donating character of the methyl groups on the two 4,4'-dimethyl-2,2'-bipyridine ligands, localizes the lowest unoccupied molecular orbitals (LUMO) of the complex, which reside on the phosphonated ligand,¹⁴ close to the metal oxide surface. This arrangement can promote rapid electron

injection and thus minimize the potentially parasitic effects of O₂. Note that the oxidation potential of excited RuP²⁹ is sufficiently negative to inject an electron into the conduction band of HCA₂Nb₃O₁₀,³⁰ suggesting that the oxidative quenching process can occur upon photoexcitation (Figure S9). The resulting one-electron-oxidized RuP can also potentially receive an electron from an electron donor such as I⁻ to regenerate its ground state.

The amount of RuP adsorbed was determined from the difference in the MLCT absorption in UV–visible absorption spectra before and after the adsorption procedure. Almost quantitative adsorption of RuP was observed up to a loading of 15 μmol g⁻¹, regardless of whether Al₂O₃ had been deposited on the nanosheets (Figure S10). This loading corresponds to approximately 30% coverage of the Pt(in)/HCA₂Nb₃O₁₀ surface, as calculated from the specific surface area of Pt(in)/HCA₂Nb₃O₁₀ (37 m² g⁻¹) and the diameter of the RuP molecule (12.3 Å). The maximum amount of RuP adsorbed on HCA₂Nb₃O₁₀ nanosheets was ca. 5 times higher than that on layered bulk HCA₂Nb₃O₁₀ that had not been exfoliated and restacked (Figure S10), demonstrating the advantage of using a nanosheet material that has higher surface area for dye adsorption.

Figure 3A shows UV–visible diffuse reflectance spectra of Al₂O₃/Pt(in)/HCA₂Nb₃O₁₀ before and after RuP adsorption. A new absorption band, which is characteristic of the MLCT absorption of RuP, appeared in the visible region after dye adsorption. The peak position was close to that of the molecule in aqueous solution, suggesting that there is almost no ground state electronic interaction between RuP and Al₂O₃/Pt(in)/HCA₂Nb₃O₁₀.

As mentioned above, electron injection from RuP to HCA₂Nb₃O₁₀ is the primary step in driving the dye-sensitized

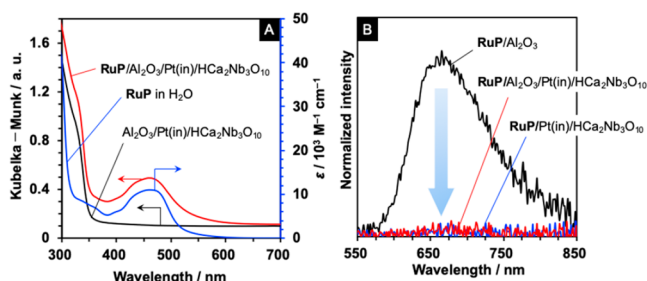


Figure 3. Spectroscopic characterization. (A) UV–visible DRS of $\text{Al}_2\text{O}_3/\text{Pt}(\text{in})/\text{HfCa}_2\text{Nb}_3\text{O}_{10}$ and RuP ($15 \mu\text{mol g}^{-1}$)/ $\text{Al}_2\text{O}_3/\text{Pt}(\text{in})/\text{HfCa}_2\text{Nb}_3\text{O}_{10}$. Absorption spectrum of RuP in H_2O is also shown. (B) Steady-state emission spectra of $\text{RuP}/\text{Al}_2\text{O}_3$, $\text{RuP}/\text{Al}_2\text{O}_3/\text{Pt}(\text{in})/\text{HfCa}_2\text{Nb}_3\text{O}_{10}$, and $\text{RuP}/\text{Pt}(\text{in})/\text{HfCa}_2\text{Nb}_3\text{O}_{10}$ suspended in H_2O saturated with Ar. Excitation wavelength was 460 nm.

photocatalytic water splitting system. The excited-state dye-to-semiconductor electron injection process can be monitored by means of emission spectroscopy.^{12–14,31,32} Al_2O_3 powder was also used as a reference; in this case, the electron injection event should not occur between RuP and Al_2O_3 because Al_2O_3 is a wide band gap insulator. As shown in Figure 3B, RuP on Al_2O_3 exhibited an emission peak at around 670 nm, giving a 4.1% emission quantum yield. In contrast, the emission was almost completely quenched on $\text{Al}_2\text{O}_3/\text{Pt}(\text{in})/\text{HfCa}_2\text{Nb}_3\text{O}_{10}$ due to excited state electron transfer from RuP to the $\text{HfCa}_2\text{Nb}_3\text{O}_{10}$ nanosheet. The emission quantum yield for RuP on $\text{Al}_2\text{O}_3/\text{Pt}(\text{in})/\text{HfCa}_2\text{Nb}_3\text{O}_{10}$ was 0.2%, meaning that more than 90% of the photoexcited RuP molecules were oxidatively quenched by $\text{Al}_2\text{O}_3/\text{Pt}(\text{in})/\text{HfCa}_2\text{Nb}_3\text{O}_{10}$. One might anticipate that the deposition of insulating Al_2O_3 would have a negative impact on the electron injection process. However, the emission quantum yield of RuP on $\text{Pt}(\text{in})/\text{HfCa}_2\text{Nb}_3\text{O}_{10}$ without Al_2O_3 was almost identical (0.2%) to that with Al_2O_3 deposition.

Z-Scheme Water Splitting Using $\text{RuP}/\text{Al}_2\text{O}_3/\text{Pt}(\text{in})/\text{HfCa}_2\text{Nb}_3\text{O}_{10}$. $\text{RuP}/\text{Al}_2\text{O}_3/\text{Pt}(\text{in})/\text{HfCa}_2\text{Nb}_3\text{O}_{10}$ nanosheets were examined as the H_2 evolution photocatalyst in Z-scheme water splitting, in combination with $\text{PtO}_x/\text{H}-\text{Cs}-\text{WO}_3$, which works as an O_2 evolution photocatalyst under visible light in the presence of an I_3^-/I^- redox mediator.³³ As listed in Table 1 (also in Figure S11), nearly stoichiometric H_2 and O_2 evolution was observed under visible light irradiation. The turnover number for H_2 evolution (TON_{H_2}) after 5 h irradiation based on the amount of RuP initially adsorbed exceeded 1200, confirming the catalytic production of H_2 in the reaction. No reaction took place without RuP or visible light irradiation. Moreover, simultaneous production of H_2 and

O_2 was not achieved in the absence of either $\text{RuP}/\text{Al}_2\text{O}_3/\text{Pt}(\text{in})/\text{HfCa}_2\text{Nb}_3\text{O}_{10}$, $\text{PtO}_x/\text{H}-\text{Cs}-\text{WO}_3$, or the I_3^-/I^- redox mediator. These results indicate that overall water splitting in a Z-scheme was realized by combining $\text{RuP}/\text{Al}_2\text{O}_3/\text{Pt}(\text{in})/\text{HfCa}_2\text{Nb}_3\text{O}_{10}$ and $\text{PtO}_x/\text{H}-\text{Cs}-\text{WO}_3$ as H_2 and O_2 evolution photocatalysts, respectively, where electron transfer between the two photocatalysts was mediated by the I_3^-/I^- redox couple. It should be noted that the presence of Al_2O_3 in the H_2 evolution photocatalyst was essential to obtaining high activity; the Al_2O_3 -containing material showed 20 times higher initial activity than the same material without Al_2O_3 (Table 1, entry 2). The effect of Al_2O_3 will be discussed in a later section.

The performance of the Z-scheme water splitting system containing $\text{RuP}/\text{Al}_2\text{O}_3/\text{Pt}(\text{in})/\text{HfCa}_2\text{Nb}_3\text{O}_{10}$ nanosheets was compared with analogous systems based on unexfoliated, bulk $\text{HfCa}_2\text{Nb}_3\text{O}_{10}$ and $\text{H}_2\text{K}_2\text{Nb}_6\text{O}_{17}$, the latter of which has been previously studied in nonsacrificial dye-sensitized systems.²² Here the same Al_2O_3 deposition, $\text{PtO}_x/\text{H}-\text{Cs}-\text{WO}_3$ photocatalyst, and an I_3^-/I^- redox mediator were employed. As listed in Table 1, the nanosheet-based system (entry 1) exhibited approximately 4 and 2 times higher activity than those of bulk $\text{HfCa}_2\text{Nb}_3\text{O}_{10}$ (entry 4) and $\text{H}_2\text{K}_2\text{Nb}_6\text{O}_{17}$ (entry 5), respectively. One of the reasons for the higher activity could be the higher loading of RuP on $\text{HfCa}_2\text{Nb}_3\text{O}_{10}$ nanosheets. Interestingly, the photocatalytic performance of the $\text{HfCa}_2\text{Nb}_3\text{O}_{10}$ nanosheet system was still higher than that of the bulk analogues even if the same amount of RuP was employed (entry 3), demonstrating the unique behavior of the nanosheet material as a component of a dye-sensitized Z-scheme for overall water splitting.

Abe et al. have reported that a similar Z-scheme system can be constructed with Pt-intercalated layered bulk $\text{H}_2\text{K}_2\text{Nb}_6\text{O}_{17}$ sensitized by coumarin dyes that have an oligothiophene moiety in their structure, in combination with an O_2 evolution photocatalyst (IrO_2 and Pt co-loaded WO_3) and an I_3^-/I^- redox couple.²² According to that study, the best performing system gave a TON_{H_2} of 513 (64 h), which corresponds to a turnover frequency (TOF_{H_2}) of 8 h^{-1} . Therefore, the present nanosheet-based system showed more than a 9-fold increase in durability and 245 times higher efficiency for H_2 production than the previously reported system. The estimated apparent quantum yield of the optimized system for overall water splitting was ca. 2.4% at 420 nm, which was higher than the value recorded under identical conditions in a similar Z-scheme system constructed from another visible-light-responsive photocatalyst, Pt-loaded, Cr/Ta-codoped SrTiO_3 (1.5%).³³ The solar-to-hydrogen energy conversion efficiency

Table 1. Photocatalytic Activities of RuP -Sensitized $\text{HfCa}_2\text{Nb}_3\text{O}_{10}$ Nanosheets, Bulk $\text{HfCa}_2\text{Nb}_3\text{O}_{10}$, and $\text{H}_2\text{K}_2\text{Nb}_6\text{O}_{17}$ in Z-Scheme Water Splitting^a

entry	H_2 evolution photocatalyst	adsorbed RuP ($\mu\text{mol g}^{-1}$)	evolved gases ^b (μmol)			
			H_2	O_2	TON_{H_2}	TOF_{H_2} (h^{-1})
1	$\text{RuP}/\text{Al}_2\text{O}_3/\text{Pt}(\text{in})/\text{HfCa}_2\text{Nb}_3\text{O}_{10}$ (nanosheet)	15	189.9	82.6	1260	440
2	$\text{RuP}/\text{Pt}(\text{in})/\text{HfCa}_2\text{Nb}_3\text{O}_{10}$ (nanosheet)	15	12.9	7.1	43	12
3	$\text{RuP}/\text{Al}_2\text{O}_3/\text{Pt}(\text{in})/\text{HfCa}_2\text{Nb}_3\text{O}_{10}$ (nanosheet)	3	137.3	72.9	4580	1960
4	$\text{RuP}/\text{Al}_2\text{O}_3/\text{Pt}(\text{in})/\text{HfCa}_2\text{Nb}_3\text{O}_{10}$ (bulk)	3	46.6	13.2	1550	570
5	$\text{RuP}/\text{Al}_2\text{O}_3/\text{Pt}(\text{in})/\text{H}_2\text{K}_2\text{Nb}_6\text{O}_{17}$ (bulk)	3	108.2	51.9	3600	1530

^aReaction conditions: catalyst, RuP -sensitized semiconductor, 20 mg; $\text{PtO}_x/\text{H}-\text{Cs}-\text{WO}_3$, 50 mg; reactant solution, 5 mM aqueous NaI (100 mL, pH 4); light source, xenon lamp (300 W) with a cold mirror (CM-1) and a cutoff filter (L42). ^bTotal amount after 5 h irradiation.

of this Z-scheme system was approximately 0.03% (see Figure S12 for detail).

Note that the degradation of activity occurred in the system after a long irradiation time. The deactivation can be attributed to partial desorption of RuP from Al₂O₃/Pt(in)/HCa₂Nb₃O₁₀ and/or decomposition (see Figure S13 for detail). Ru(II) tris-diimine complexes have been reported to undergo ligand exchange to produce Ru(II) bis-diimine complexes during homogeneous photocatalytic reactions in aqueous solutions, resulting in the termination of photocatalysis.³⁴ The characteristic absorption of the decomposed Ru(II) photosensitizer at $\lambda_{\text{max}} = 495$ nm, which is at a longer wavelength than the original RuP photosensitizer ($\lambda_{\text{max}} = 460$ nm), was observed in the solution after photocatalysis. This decomposition process would possibly be suppressed by using a more stable photosensitizer such as an Ir(III) complex or a metal-porphyrin.

Role of Al₂O₃ Loading on Pt(in)/HCa₂Nb₃O₁₀ Nanosheets in the Z-Scheme Overall Water Splitting. The results described above highlight the utility of a suitably modified nanosheet material in a Z-scheme for water splitting, and also indicate a large effect of the Al₂O₃ modifier in increasing the efficiency. Emission spectroscopy measurements showed that introducing Al₂O₃ did not produce a noticeable change in the electron injection efficiency from the excited state of RuP to the HCa₂Nb₃O₁₀ nanosheets (Figure 3B), suggesting that the beneficial effect of the Al₂O₃ modifier derives from reaction steps following electron injection. Given the reaction scheme shown in Figure 1, there are two main possibilities for the role of Al₂O₃: (1) it promotes the reduction of oxidized RuP by I⁻ and/or (2) it suppresses back electron transfer from the conduction band of HCa₂Nb₃O₁₀ nanosheets to oxidized RuP and/or I₃⁻ (or I₂^{•-}).

To obtain a deeper insight on the role of Al₂O₃, transient diffuse reflectance spectra were measured in aqueous suspensions containing RuP/Pt(in)/HCa₂Nb₃O₁₀ with and without Al₂O₃. Following a laser flash at 532 nm to selectively photoexcite the RuP sensitizer, bleaching of the MLCT absorption of ground-state RuP was observed. It has been reported that ground state bleaching of [Ru(bpy)₃]²⁺ occurs within 1 ps after photoexcitation.³⁵ The bleaching monitored at 460 nm gradually recovered over a few ms in H₂O (i.e., in the absence of NaI) because of back electron transfer from the conduction band of HCa₂Nb₃O₁₀ to oxidized RuP (Figure S14), and almost no change was seen in the recovery profiles upon Al₂O₃ deposition. It should be noted that the recovery of the RuP bleaching was not completed even after a few ms of laser excitation, which was 1 order of magnitude slower than those reported in previous dye-sensitized oxide systems constructed with layered oxides (several hundreds of μs).^{9,17,21}

On the other hand, the recovery process became 2 orders of magnitude faster in the presence of NaI due to the forward electron transfer from I⁻ to oxidized RuP (Figure 4). The profiles could be fitted by a double-exponential function, showing that the lifetimes were shortened by Al₂O₃ deposition (see the inset of Figure 4). Furthermore, decay profiles of oxidized I⁻ species could also be traced by monitoring transient absorbance signal at 380 nm.^{9,17} In this experiment, no noticeable change was identified regardless of Al₂O₃ deposition (Figure S15), indicating that Al₂O₃ had no impact on the suppression of I₃⁻ reduction. This conclusion is also supported by the results of the H₂ evolution reaction in the presence of I₂ (Figure S16).

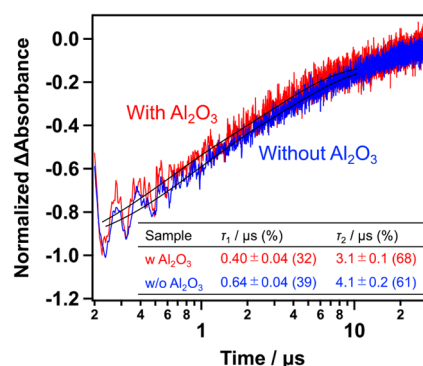


Figure 4. Time-dependent absorbance change in transient absorption spectra of RuP-sensitized HCa₂Nb₃O₁₀ nanosheets with and without Al₂O₃ recorded in an aqueous NaI suspension (5 mM, pH 4) and monitored at 475 nm. The inset summarizes lifetimes for recovery processes monitored at 475 nm.

These results indicate that Al₂O₃ facilitates forward electron transfer from I⁻ to oxidized RuP, but does not prevent undesirable back electron transfer events. Choi et al. have reported that modification of TiO₂ by an Al₂O₃ overlayer retards the charge recombination between injected electrons in the conduction band of TiO₂ and the oxidized dye in a dye-sensitized H₂ evolution system.²¹ Obviously, the effect of Al₂O₃ modification on the HCa₂Nb₃O₁₀ nanosheets was different from that of TiO₂, as Al₂O₃ on the nanosheets did not suppress the back electron transfer events but promoted forward electron transfer (i.e., the regeneration of oxidized RuP). The origin of the enhanced rate of reduction of oxidized RuP by I⁻ can be reasonably explained in terms of a change in the surface charge of Pt(in)/HCa₂Nb₃O₁₀ after the Al₂O₃ deposition. ζ -potential measurements revealed that the surface of the Pt(in)/HCa₂Nb₃O₁₀ nanosheets was negatively charged over the entire pH range examined (Figure S17), consistent with the result obtained with HCa₂Nb₃O₁₀ nanosheets.¹² However, the Al₂O₃-containing material was more positively charged at pH < 4. It is therefore likely that the more positively charged Al₂O₃/Pt(in)/HCa₂Nb₃O₁₀ surface attracted I⁻ ions to its surface, thereby promoting the regeneration of RuP.

CONCLUSIONS

In this study, we have demonstrated the enhanced activity of restacked calcium niobate nanosheets as the hydrogen-evolving component of a dye-sensitized photocatalytic system for overall water splitting. Al₂O₃ modified, Pt intercalated, and dye-sensitized HCa₂Nb₃O₁₀ nanosheets were highly active for visible light water splitting in a combination with PtO_x/H-Cs-WO₃ as the O₂ evolving photocatalyst. The dye-based turnover number and turnover frequency for H₂ evolution reached 4580 and 1960 h⁻¹, respectively, which were 9 and 245 times higher than a previous report by Abe and co-workers using Pt-intercalated layered bulk H₂K₂Nb₆O₁₇ and a coumarin dye. These values are the highest yet among dye-sensitized overall water splitting systems. Electron transfer processes between the dye, nanosheet, and electron donor were investigated in detail by transient absorption spectroscopy, which showed that Al₂O₃ promoted the reduction of oxidized RuP by I⁻. Although surface modification techniques have been used in dye-sensitized photocatalysis to prevent back electron transfer, the effect of Al₂O₃ observed here is

unprecedented and may offer new insight into the design of more efficient dye-sensitized photocatalysts.

EXPERIMENTAL SECTION

Preparation of $\text{Al}_2\text{O}_3/\text{Pt}(\text{in})/\text{HCa}_2\text{Nb}_3\text{O}_{10}$ Nanosheet. A TBA^+ -stabilized $\text{Ca}_2\text{Nb}_3\text{O}_{10}^-$ nanosheet suspension was prepared according to previous reports.^{36,37} First, layered bulk $\text{KCa}_2\text{Nb}_3\text{O}_{10}$ was synthesized by solid state reaction. K_2CO_3 ($\geq 99.5\%$, Kanto Chemical Co.), CaCO_3 ($\geq 99.5\%$, Kanto Chemical Co.), and Nb_2O_5 ($\geq 99.95\%$, Kanto Chemical Co.) were mixed in an agate mortar and pestle in the presence of a small amount of methanol. The mixture was preheated at 1123 K for 1 h in an Al_2O_3 crucible, followed by final calcination at 1423 K for 10 h. The ratio of K, Ca, and Nb in the starting mixture was 1.1:2:3, where 10% excess K was added to compensate for loss during calcination. The obtained $\text{KCa}_2\text{Nb}_3\text{O}_{10}$ was then stirred in an aqueous HNO_3 solution (1 M, 69–70%, Kanto Chemical Co.) for 3 days to exchange K^+ into H^+ , followed by washing with H_2O thoroughly and drying at 343 K in an oven. Finally, the $\text{HCa}_2\text{Nb}_3\text{O}_{10}$ was stirred in an aqueous TBA^+OH^- solution (Aldrich Chemical Co., 40 wt % in H_2O) for 1 week, in which a stoichiometric amount of TBA^+OH^- to $\text{HCa}_2\text{Nb}_3\text{O}_{10}$ was used, to obtain a colloidal nanosheet suspension. Unreacted $\text{HCa}_2\text{Nb}_3\text{O}_{10}$ was removed by decantation.

Pt was deposited on $\text{HCa}_2\text{Nb}_3\text{O}_{10}$ restacked nanosheets according to our previous report.²⁵ An aqueous solution containing $[\text{Pt}(\text{NH}_3)_4]\text{Cl}_2$ (1 mM, Pt 1 wt % with respect to $\text{Ca}_2\text{Nb}_3\text{O}_{10}^-$, Wako Pure Chemicals) was added dropwise into the $\text{TBA}^+/\text{Ca}_2\text{Nb}_3\text{O}_{10}^-$ nanosheet suspension (5 g L^{-1}) and the suspension was stirred for 1 day to adsorb the Pt precursor onto $\text{Ca}_2\text{Nb}_3\text{O}_{10}^-$ based on their electrostatic interaction. The resulting nanosheet was restacked by adding an aqueous HCl solution (2 M, 35.0–37.0%, Kanto Chemical Co.). The precipitate was washed with H_2O repeatedly, and dried at 343 K in an oven, followed by H_2 reduction at 473 K for 1 h under H_2 flow of 20 mL min^{-1} . The Pt(in-out)/ $\text{HCa}_2\text{Nb}_3\text{O}_{10}$ obtained in this way was stirred in a mixture of aqueous concentrated HNO_3 and HCl solutions (1:3 v/v) at the boiling temperature for 15 min to dissolve Pt on the external surface of $\text{HCa}_2\text{Nb}_3\text{O}_{10}$.

Al_2O_3 was deposited by a sol-gel method on Pt(in)/ $\text{HCa}_2\text{Nb}_3\text{O}_{10}$ as follows. Typically, 100 mg of Pt(in)/ $\text{HCa}_2\text{Nb}_3\text{O}_{10}$ was suspended in 20 mL of ethanol ($\geq 99.5\%$, Kanto Chemical Co.) containing 100 μL of aqueous H_2SO_4 ($\geq 96.0\%$, Kanto Chemical Co.) solution (0.1 M) and an appropriate amount of aluminum isopropoxide ($\geq 98.0\%$, TCI). The suspension was subjected to sonication for 30 min, followed by stirring for 1 day. The resulting powder was washed with water and dried at room temperature under a vacuum. The preparation scheme is depicted in Scheme 1.

Preparation of $\text{Al}_2\text{O}_3/\text{Pt}(\text{in})/\text{Bulk HCa}_2\text{Nb}_3\text{O}_{10}$ and $\text{Al}_2\text{O}_3/\text{Pt}(\text{in})/\text{H}_2\text{K}_2\text{Nb}_6\text{O}_{17}$. Layered bulk $\text{HCa}_2\text{Nb}_3\text{O}_{10}$ was dispersed in an aqueous $[\text{Pt}(\text{NH}_3)_4]\text{Cl}_2$ solution (Pt 1 wt % with respect to $\text{HCa}_2\text{Nb}_3\text{O}_{10}$) and stirred for 3 days at room temperature. The resulting powder was washed with H_2O , dried at 343 K in an oven, and heated at 473 K for 1 h under a flow of H_2 (20 mL min^{-1}).

Pt(in)/ $\text{H}_2\text{K}_2\text{Nb}_6\text{O}_{17}$ was prepared according to a previous report with some modifications.²² $\text{K}_4\text{Nb}_6\text{O}_{17}$ was synthesized by solid state reaction from a mixture of K_2CO_3 and Nb_2O_5 at 1473 K for 15 min in an Al_2O_3 crucible. 10% excess K was added to compensate for loss during calcination. The as-synthesized $\text{K}_4\text{Nb}_6\text{O}_{17}$ was ground into a powder, dispersed in an aqueous $[\text{Pt}(\text{NH}_3)_4]\text{Cl}_2$ solution (Pt 1 wt % with respect to $\text{K}_4\text{Nb}_6\text{O}_{17}$), and stirred for 3 days at room temperature. The resulting powder was washed with H_2O , dried at 343 K in an oven, and heated at 473 K for 1 h under a H_2 flow (20 mL min^{-1}). The resulting Pt-deposited $\text{K}_4\text{Nb}_6\text{O}_{17}$ was stirred in an aqueous HCl solution (0.5 M) for 3 days to promote the H^+ -exchange reaction, washed with H_2O , and dried at 343 K in an oven.

Removal of Pt on the external surface and deposition of Al_2O_3 were conducted in the same manner as for the $\text{Al}_2\text{O}_3/\text{Pt}(\text{in})/\text{HCa}_2\text{Nb}_3\text{O}_{10}$ nanosheet samples.

Synthesis and Adsorption of Ru(II) Photosensitizer. $[\text{Ru}(4,4'-(\text{CH}_3)_2\text{-bpy})_2(4,4'-(\text{PO}_3\text{H}_2)_2\text{-bpy})]\text{Cl}_2$, referred to as RuP, was

synthesized according to a previous report with some modifications.²⁹ Adsorption of RuP onto the metal oxide surface was carried out as follows. 50 mg of solid material was suspended in an appropriate volume of aqueous RuP solution (50 μM). The pH was adjusted to 2 by addition of an aqueous HCl solution. The suspension was stirred for 15 h at room temperature in the dark, followed by filtration, washing with H_2O , and drying at room temperature under a vacuum. The adsorbed amount of RuP was estimated from a difference in the MLCT absorption in the UV-vis absorption spectrum before and after adsorption using a molar absorption coefficient $\epsilon = 10\,200\text{ M}^{-1}\text{ cm}^{-1}$.

Preparation of $\text{PtO}_x/\text{H-Cs-WO}_3$. $\text{PtO}_x/\text{H-Cs-WO}_3$ was prepared according to previous reports with some modifications.^{33,38} Large particles of WO_3 ($\geq 99.99\%$, Kojundo Chemical Co.) heated at 973 K were collected by sonication and decantation. Then, 0.5 wt % Pt was deposited on the WO_3 by an impregnation method using H_2PtCl_6 ($\geq 98.5\%$, Kanto Chemical Co.) as a precursor, followed by heating at 823 K for 30 min in a muffle furnace. Then, Cs_2CO_3 (Cs 1 wt %, $\geq 98.0\%$, Kanto Chemical Co.) was impregnated into the PtO_x/WO_3 and heated at 773 K for 10 min in air. The resulting powder was stirred in 1 M aqueous H_2SO_4 solution for 30 min, filtered, washed with H_2O , and dried at 343 K in an oven.

Characterization. XRD patterns were recorded on a Rigaku MiniFlex600 powder diffractometer employing $\text{Cu K}\alpha$ radiation and operating at 15 mA and 40 kV. UV-visible absorption and diffuse reflectance spectra were obtained using a spectrophotometer (V-565, JASCO). For diffuse reflectance measurements, an integrating sphere and Spectralon reference sample were used. SEM images were obtained using a Hitachi SU-9000 field emission scanning electron microscope. XPS spectra were acquired using an ESCA-3400 X-ray photoelectron spectrometer (Shimadzu). The binding energies were calibrated by referencing the C 1s peak (284.6 eV) for each sample. FT-IR spectra were recorded using a FT/IR-6600 spectrometer (JASCO) with a KBr pellet. The Brunauer-Emmett-Teller (BET) surface area was determined from N_2 adsorption isotherms using a BELSORP-mini instrument (MicrotracBEL) at liquid nitrogen temperature. Samples were heated at 423 K for 1 h under a vacuum prior to the measurements. ζ -potentials of Pt(in)/ $\text{HCa}_2\text{Nb}_3\text{O}_{10}$ nanosheets with and without Al_2O_3 were measured using a Zeta-potential & Particle size Analyzer (OTSUKA ELECTRONICS, ELSZ-1PL). Aqueous HCl or NaOH solutions were used to adjust pH.

For the STEM observations, a Titan Cubed microscope (Thermo Fisher Scientific) equipped with spherical aberration correctors (CEOS) and an EDS detector (Oxford Instruments, X-Max^N 100TLE) was used at an acceleration voltage of 300 kV. The convergence semiangle of the incident probe was 18 mrad. The inner and outer detection semiangles of the ADF detector were 46 and 200 mrad, respectively. The incident probe current was set to 17 pA.

Emission Quantum Yield Measurement. Emission quantum yields of RuP on solid samples were measured using a Quantaurus-QY Plus (Hamamatsu, C13534-11). The RuP-adsorbed powder suspension was placed in a measurement cell made of Pyrex glass and bubbled with Ar for 30 min prior to the measurements. The excitation wavelength was 460 nm. Al_2O_3 (40–50 nm, Wako Pure Chemicals), heated at 773 K for 1 h in a furnace prior to RuP adsorption, was used as a reference.

Transient Absorption Spectroscopy. Transient absorption spectroscopy measurements were performed using an enVISION transient absorption system (Magnitude Instruments, State College, PA), which consisted of a pulsed, frequency doubled (532 nm) Nd:YAG laser as the excitation source and a xenon lamp as the probe light source. The probe light source was dispersed through a monochromator and detected with a photovoltaic detector. Approximately 5 mg of RuP sensitized $\text{HCa}_2\text{Nb}_3\text{O}_{10}$ nanosheet sample was dispersed in an aqueous NaI solution (5 mM, 4 mL, $\geq 99.9\%$, Fisher Science Education) or pure water in a quartz cuvette and spectra were recorded in diffuse reflectance mode. The suspension was purged with Ar for at least for 20 min prior to

experiments. 0.1 M NaI was used to observe a transient decay of oxidized I⁻ species.

Photocatalytic Reactions. Photocatalytic reactions were performed in a glass closed circulation system. A top irradiation type reaction cell made of Pyrex glass was used, combined with a cooling water bath to maintain the temperature of the reactor at approximately 293 K throughout the reaction. For Z-scheme water splitting, 20 mg of a H₂-evolution photocatalyst (e.g., RuP/Al₂O₃/Pt(in)/HCa₂Nb₃O₁₀) and 50 mg of PtO_x/H-Cs-WO₃ were suspended in 5 mM aqueous NaI (≥99.5%, Kanto Chemical Co.) solution (100 mL) unless otherwise stated. The pH of reaction solution was adjusted to 4 by adding 0.1 M aqueous H₂SO₄ solution. For the H₂ evolution half reaction, 20 mg of photocatalyst was suspended in an aqueous 100 mL solution containing 10 mM NaI with and without addition of I₂ (1 mM). The pH of the reaction solution was adjusted to 4 by addition of aqueous HCl solution. After degassing the reaction cell, a small amount (ca. 1 kPa) of argon gas was introduced and the suspension was irradiated using a 300 W xenon lamp (Cermax, PE300BF). The irradiation wavelength was controlled by using a CM-1 cold mirror and a L42 cutoff filter. The evolved gases were analyzed by gas chromatography (Shimadzu, GC-8A with a TCD detector and an MS-5A column, argon carrier gas). The turnover number for H₂ evolution (TON_{H₂}) was calculated according to the following equation:²²

$$\text{TON}_{\text{H}_2} = \text{Amount of evolved H}_2 \times 2 / \text{Amount of adsorbed RuP}$$

The turnover frequency for H₂ evolution (TOF_{H₂}) was calculated by dividing the TON_{H₂} recorded at 1 h by time.

The apparent quantum yield (AQY) for H₂ evolution was measured using the same experimental setup with a band-pass filter (λ = 420 nm), and was estimated as

$$\text{AQY} (\%) = A \times R / I \times 100$$

where A, R, and I represent the reaction coefficient, the H₂ evolution rate, and the rate of incident photons, respectively. The total number of incident photons (ca. 45.2 mW) was measured using a calibrated silicon photodiode.

Water Formation Reaction. The recombination reaction between H₂ and O₂ was studied in a glass closed circulation system. Twenty mg of catalyst was dispersed in pure water (100 mL), and the reaction solution was thoroughly degassed. Then, approximately 200 μmol of H₂ and 100 μmol of O₂ were introduced into the glass closed circulation system, and the recombination reaction was carried out under dark conditions. The amount of each gas was analyzed by gas chromatography.

■ ASSOCIATED CONTENT

SI Supporting Information

The Supporting Information is available free of charge at <https://pubs.acs.org/doi/10.1021/jacs.0c02053>.

Additional reaction and characterization data (Figure S1–S17) (PDF)

■ AUTHOR INFORMATION

Corresponding Authors

Thomas E. Mallouk – Department of Chemistry, University of Pennsylvania, Philadelphia, Pennsylvania 19104, United States; International Center for Materials Nanoarchitectonics (WPI-MANA), National Institute for Materials Science (NIMS), Tsukuba, Ibaraki 305-0044, Japan; orcid.org/0000-0003-4599-4208; Email: mallouk@sas.upenn.edu

Kazuhiro Maeda – Department of Chemistry, School of Science, Tokyo Institute of Technology, Meguro-ku, Tokyo 152-8550, Japan; orcid.org/0000-0001-7245-8318; Email: maedak@chem.titech.ac.jp

Authors

Takayoshi Oshima – Department of Chemistry, School of Science, Tokyo Institute of Technology, Meguro-ku, Tokyo 152-8550, Japan; Japan Society for the Promotion of Science, Chiyoda-ku, Tokyo 102-0083, Japan

Shunta Nishioka – Department of Chemistry, School of Science, Tokyo Institute of Technology, Meguro-ku, Tokyo 152-8550, Japan; Japan Society for the Promotion of Science, Chiyoda-ku, Tokyo 102-0083, Japan; Department of Chemistry, University of Pennsylvania, Philadelphia, Pennsylvania 19104, United States; orcid.org/0000-0003-1977-7058

Yuka Kikuchi – Graduate School of Science and Technology, Niigata University, Niigata 950-2181, Japan

Shota Hirai – Department of Chemistry, School of Science, Tokyo Institute of Technology, Meguro-ku, Tokyo 152-8550, Japan

Kei-ichi Yanagisawa – Research Center for Advanced Measurement and Characterization, National Institute for Materials Science (NIMS), Tsukuba, Ibaraki 305-0044, Japan

Miharu Eguchi – Research Center for Functional Materials, National Institute for Materials Science (NIMS), Tsukuba, Ibaraki 305-0044, Japan; orcid.org/0000-0002-4007-7438

Yugo Miseki – Research Center for Photovoltaics (RCPV) and Global Zero Emission Research Center (GZR), National Institute of Advanced Industrial Science and Technology (AIST), Tsukuba, Ibaraki 305-8565, Japan; orcid.org/0000-0002-3208-9834

Toshiyuki Yokoi – Nanospace Catalysis Unit, Institute of Innovative Research, Tokyo Institute of Technology, Midori-ku, Yokohama 226-8503, Japan

Tatsuto Yui – Graduate School of Science and Technology, Niigata University, Niigata 950-2181, Japan; orcid.org/0000-0002-7526-3521

Koji Kimoto – Research Center for Advanced Measurement and Characterization, National Institute for Materials Science (NIMS), Tsukuba, Ibaraki 305-0044, Japan

Kazuhiro Sayama – Research Center for Photovoltaics (RCPV) and Global Zero Emission Research Center (GZR), National Institute of Advanced Industrial Science and Technology (AIST), Tsukuba, Ibaraki 305-8565, Japan; orcid.org/0000-0003-1847-5242

Osamu Ishitani – Department of Chemistry, School of Science, Tokyo Institute of Technology, Meguro-ku, Tokyo 152-8550, Japan; orcid.org/0000-0001-9557-7854

Complete contact information is available at: <https://pubs.acs.org/doi/10.1021/jacs.0c02053>

Notes

The authors declare no competing financial interest.

■ ACKNOWLEDGMENTS

This work was supported by a Grant-in-Aid for Scientific Research on the Innovative Area Mixed Anions (JP16H06440, JP16H06441, JP17H05477, and JP19H04691), for Challenging Research (Exploratory) (JP17K19169), and for Scientific Research (B) (JP19H02511) (JSPS). T.O. and S.N. wish to acknowledge support by a JSPS Fellowship for Young Scientists (JP16J10084 and JP18J10457). T.Y. acknowledges support from the Institute of Materials and Systems for Sustainability, Nagoya University and MEXT/JSPS KAKENHI JP17K19173. T.E.M. and S.N. acknowledge support from the

Office of Basic Energy Sciences, Division of Chemical Sciences, Geosciences, and Energy Biosciences, Department of Energy, under contract DE-SC0019781. K.M. wishes to thank the ENEOS Hydrogen Trust Fund.

REFERENCES

- (1) Gerischer, H. Electrochemical Techniques for the Study of Photosensitization*. *Photochem. Photobiol.* **1972**, *16*, 243–260.
- (2) Hashimoto, K.; Kawai, T.; Sakata, T. Efficient Hydrogen Production from Water by Visible Light Excitation of Fluorescein-Type Dyes in the Presence of a Redox Catalyst and a Reducing Agent. *Chem. Lett.* **1983**, *12*, 709–712.
- (3) Abe, R.; Hara, K.; Sayama, K.; Domen, K.; Arakawa, H. Steady Hydrogen Evolution from Water on Eosin Y-Fixed TiO₂ Photocatalyst Using a Silane-Coupling Reagent under Visible Light Irradiation. *J. Photochem. Photobiol., A* **2000**, *137*, 63–69.
- (4) Park, H.; Bae, E.; Lee, J. J.; Park, J.; Choi, W. Effect of the Anchoring Group in Ru-Bipyridyl Sensitizers on the Photoelectrochemical Behavior of Dye-Sensitized TiO₂ Electrodes: Carboxylate Versus Phosphonate Linkages. *J. Phys. Chem. B* **2006**, *110*, 8740–8749.
- (5) Bae, E.; Choi, W. Effect of the Anchoring Group (Carboxylate vs Phosphonate) in Ru-Complex-Sensitized TiO₂ on Hydrogen Production under Visible Light. *J. Phys. Chem. B* **2006**, *110*, 14792–14799.
- (6) Kim, W.; Tachikawa, T.; Majima, T.; Li, C.; Kim, H.-J.; Choi, W. Tin-Porphyrin Sensitized TiO₂ for the Production of H₂ under Visible Light. *Energy Environ. Sci.* **2010**, *3*, 1789–1795.
- (7) Kobayashi, A.; Watanabe, S.; Yoshida, M.; Kato, M. Importance of the Molecular Orientation of an Iridium(III)-Heteroleptic Photosensitizer Immobilized on TiO₂ Nanoparticles. *ACS Appl. Energy Mater.* **2018**, *1*, 2882–2890.
- (8) Kim, Y. I.; Salim, S.; Hug, M. J.; Mallouk, T. E. Visible-Light Photolysis of Hydrogen Iodide Using Sensitized Layered Semiconductor Particles. *J. Am. Chem. Soc.* **1991**, *113*, 9561–9563.
- (9) Kim, Y. I.; Atherton, S. J.; Brigham, E. S.; Mallouk, T. E. Sensitized Layered Metal Oxide Semiconductor Particles for Photochemical Hydrogen Evolution from Nonsacrificial Electron Donors. *J. Phys. Chem.* **1993**, *97*, 11802–11810.
- (10) Park, H.; Choi, W. Visible-Light-Sensitized Production of Hydrogen Using Perfluorosulfonate Polymer-Coated TiO₂ Nanoparticles: An Alternative Approach to Sensitizer Anchoring. *Langmuir* **2006**, *22*, 2906–2911.
- (11) Maeda, K.; Eguchi, M.; Youngblood, W. J.; Mallouk, T. E. Niobium Oxide Nanoscrolls as Building Blocks for Dye-Sensitized Hydrogen Production from Water under Visible Light Irradiation. *Chem. Mater.* **2008**, *20*, 6770–6778.
- (12) Maeda, K.; Eguchi, M.; Lee, S.-H. A.; Youngblood, W. J.; Hata, H.; Mallouk, T. E. Photocatalytic Hydrogen Evolution from Hexaniobate Nanoscrolls and Calcium Niobate Nanosheets Sensitized by Ruthenium(II) Bipyridyl Complexes. *J. Phys. Chem. C* **2009**, *113*, 7962–7969.
- (13) Maeda, K.; Eguchi, M.; Youngblood, W. J.; Mallouk, T. E. Calcium Niobate Nanosheets Prepared by the Polymerized Complex Method as Catalytic Materials for Photochemical Hydrogen Evolution. *Chem. Mater.* **2009**, *21*, 3611–3617.
- (14) Maeda, K.; Sahara, G.; Eguchi, M.; Ishitani, O. Hybrids of a Ruthenium(II) Polypyridyl Complex and a Metal Oxide Nanosheet for Dye-Sensitized Hydrogen Evolution with Visible Light: Effects of the Energy Structure on Photocatalytic Activity. *ACS Catal.* **2015**, *5*, 1700–1707.
- (15) Reiser, E.; Fontecilla-Camps, J. C.; Armstrong, F. A. Catalytic Electrochemistry of a [NiFeSe]-Hydrogenase on TiO₂ and Demonstration of Its Suitability for Visible-Light Driven H₂ Production. *Chem. Commun.* **2009**, 550–552.
- (16) Reiser, E.; Powell, D. J.; Cavazza, C.; Fontecilla-Camps, J. C.; Armstrong, F. A. Visible Light-Driven H₂ Production by Hydrogenases Attached to Dye-Sensitized TiO₂ Nanoparticles. *J. Am. Chem. Soc.* **2009**, *131*, 18457–18466.
- (17) Saupe, G. B.; Mallouk, T. E.; Kim, W.; Schmehl, R. H. Visible Light Photolysis of Hydrogen Iodide Using Sensitized Layered Metal Oxide Semiconductors: The Role of Surface Chemical Modification in Controlling Back Electron Transfer Reactions. *J. Phys. Chem. B* **1997**, *101*, 2508–2513.
- (18) Shimidzu, T.; Iyoda, T.; Koide, Y. An Advanced Visible-Light-Induced Water Reduction with Dye-Sensitized Semiconductor Powder Catalyst. *J. Am. Chem. Soc.* **1985**, *107*, 35–41.
- (19) Furlong, D. N.; Wells, D.; Sasse, W. H. F. Colloidal Semiconductors in Systems for the Sacrificial Photolysis of Water: Sensitization of Titanium Dioxide by Adsorption of Ruthenium Complexes. *J. Phys. Chem.* **1986**, *90*, 1107–1115.
- (20) Vinodgopal, K.; Hua, X.; Dahlgren, R. L.; Lappin, A. G.; Patterson, L. K.; Kamat, P. V. Photochemistry of Ru(bpy)₂(dcbpy)²⁺ on Al₂O₃ and TiO₂ Surfaces. An Insight into the Mechanism of Photosensitization. *J. Phys. Chem.* **1995**, *99*, 10883–10889.
- (21) Kim, W.; Tachikawa, T.; Majima, T.; Choi, W. Photocatalysis of Dye-Sensitized TiO₂ Nanoparticles with Thin Overcoat of Al₂O₃: Enhanced Activity for H₂ Production and Dechlorination of CCl₄. *J. Phys. Chem. C* **2009**, *113*, 10603–10609.
- (22) Abe, R.; Shinmei, K.; Koumura, N.; Hara, K.; Ohtani, B. Visible-Light-Induced Water Splitting Based on Two-Step Photoexcitation between Dye-Sensitized Layered Niobate and Tungsten Oxide Photocatalysts in the Presence of a Triiodide/Iodide Shuttle Redox Mediator. *J. Am. Chem. Soc.* **2013**, *135*, 16872–16884.
- (23) Uppuluri, R.; Sen Gupta, A.; Rosas, A. S.; Mallouk, T. E. Soft Chemistry of Ion-Exchangeable Layered Metal Oxides. *Chem. Soc. Rev.* **2018**, *47*, 2401–2430.
- (24) Maeda, K.; Mallouk, T. E. Two-Dimensional Metal Oxide Nanosheets as Building Blocks for Artificial Photosynthetic Assemblies. *Bull. Chem. Soc. Jpn.* **2019**, *92*, 38–54.
- (25) Oshima, T.; Lu, D.; Ishitani, O.; Maeda, K. Intercalation of Highly Dispersed Metal Nanoclusters into a Layered Metal Oxide for Photocatalytic Overall Water Splitting. *Angew. Chem., Int. Ed.* **2015**, *54*, 2698–2702.
- (26) McGuire, G. E.; Schweitzer, G. K.; Carlson, T. A. Core Electron Binding Energies in Some Group IIIA, VB, and VIB Compounds. *Inorg. Chem.* **1973**, *12*, 2450–2453.
- (27) Hess, A.; Kemnitz, E.; Lippitz, A.; Unger, W. E. S.; Menz, D. H. ESCA, XRD, and IR Characterization of Aluminum Oxide, Hydroxyfluoride, and Fluoride Surfaces in Correlation with Their Catalytic Activity in Heterogeneous Halogen Exchange Reactions. *J. Catal.* **1994**, *148*, 270–280.
- (28) Lin, C. T.; Boettcher, W.; Chou, M.; Creutz, C.; Sutin, N. Mechanism of the Quenching of the Emission of Substituted Polypyridineruthenium(II) Complexes by Iron(III), Chromium(III), and Europium(III) Ions. *J. Am. Chem. Soc.* **1976**, *98*, 6536–6544.
- (29) Ashford, D. L.; Brennaman, M. K.; Brown, R. J.; Keinan, S.; Concepcion, J. J.; Papanikolas, J. M.; Templeton, J. L.; Meyer, T. J. Varying the Electronic Structure of Surface-Bound Ruthenium(II) Polypyridyl Complexes. *Inorg. Chem.* **2015**, *54*, 460–469.
- (30) Xu, P.; Milstein, T. J.; Mallouk, T. E. Flat-Band Potentials of Molecularly Thin Metal Oxide Nanosheets. *ACS Appl. Mater. Interfaces* **2016**, *8*, 11539–11547.
- (31) Maeda, K.; Oshima, T.; Ishitani, O. Emission Spectroscopy of a Ruthenium(II) Polypyridyl Complex Adsorbed on Calcium Niobate Lamellar Solids and Nanosheets. *Phys. Chem. Chem. Phys.* **2015**, *17*, 17962–17966.
- (32) Nishioka, S.; Yamazaki, Y.; Okazaki, M.; Sekizawa, K.; Sahara, G.; Murakoshi, R.; Saito, D.; Kuriki, R.; Oshima, T.; Hyodo, J.; Yamazaki, Y.; Ishitani, O.; Mallouk, T. E.; Maeda, K. Defect Density-Dependent Electron Injection from Excited-State Ru(II) Tris-Diimine Complexes into Defect-Controlled Oxide Semiconductors. *J. Phys. Chem. C* **2019**, *123*, 28310–28318.
- (33) Miseki, Y.; Fujiyoshi, S.; Gunji, T.; Sayama, K. Photocatalytic Water Splitting under Visible Light Utilizing I₃⁻/I⁻ and IO₃⁻/I⁻

Redox Mediators by Z-Scheme System Using Surface Treated PtO_x/WO₃ as O₂ Evolution Photocatalyst. *Catal. Sci. Technol.* **2013**, *3*, 1750.

(34) Nakada, A.; Koike, K.; Nakashima, T.; Morimoto, T.; Ishitani, O. Photocatalytic CO₂ Reduction to Formic Acid Using a Ru(II)-Re(I) Supramolecular Complex in an Aqueous Solution. *Inorg. Chem.* **2015**, *54*, 1800–1807.

(35) Wallin, S.; Davidsson, J.; Modin, J.; Hammarstrom, L. Femtosecond Transient Absorption Anisotropy Study on [Ru-(bpy)₃]²⁺ and [Ru(bpy)(py)₄]²⁺. Ultrafast Interligand Randomization of the MLCT State. *J. Phys. Chem. A* **2005**, *109*, 4697–4704.

(36) Ebina, Y.; Sasaki, T.; Harada, M.; Watanabe, M. Restacked Perovskite Nanosheets and Their Pt-Loaded Materials as Photocatalysts. *Chem. Mater.* **2002**, *14*, 4390–4395.

(37) Ebina, Y.; Sakai, N.; Sasaki, T. Photocatalyst of Lamellar Aggregates of RuO_x-Loaded Perovskite Nanosheets for Overall Water Splitting. *J. Phys. Chem. B* **2005**, *109*, 17212–17216.

(38) Miseki, Y.; Sayama, K. Photocatalytic Water Splitting Employing a [Fe(CN)₆]^{3-/4-} Redox Mediator under Visible Light. *Catal. Sci. Technol.* **2019**, *9*, 2019–2024.